Eur. Phys. J. C (2024) 84:1287
https://doi.org/10.1140/epjc/s10052-024-13646-0

THE EUROPEAN PHYSICAL JOURNAL C

Regular Article - Theoretical Physics

Screening length of a heavy quark–antiquark pair in non-commutative plasma

Ping-ping Wu[1,a], **Xiangrong Zhu**[2,b], **Zi-qiang Zhang**[3,c]

[1] School of Physics and Electronic Information Engineering, Henan Polytechnic University, Jiaozuo 454000, China
[2] School of Science, Huzhou University, Huzhou 313000, China
[3] School of Mathematics and Physics, China University of Geosciences, Wuhan 430074, China

Received: 6 October 2024 / Accepted: 24 November 2024

Abstract We investigate the screening length of a heavy quark–antiquark ($Q\bar{Q}$) pair in non-commutative $\mathcal{N} = 4$ super Yang–Mills plasma at strong coupling. We perform the analysis by computing the Wilson loop in a boosted background and consider the axis of the $Q\bar{Q}$ pair along different directions. It turns out that the inclusion of non-commutativity increases the screening length, thus enhancing the binding energy of the $Q\bar{Q}$ pair. Furthermore, the presence of non-commutativity reduces quarkonium dissociation, in agreement with previous findings of the imaginary potential and entropic force.

1 Introduction

Collisions of heavy nuclei in the lab at the Relativistic Heavy Ion Collider (RHIC) and Large Hadron Collider (LHC) are believed to produce a new state of matter, so-called quark gluon plasma (QGP) [1–3]. Extensive research has shown that QGP is strongly coupled and behaves like a nearly perfect relativistic fluid [4,5]. Therefore, the study of QGP requires strong coupling techniques. Anti-de Sitter space/conformal field theory (AdS/CFT) correspondence can relate a weakly coupled string theory in the AdS space to a strongly coupled CFT (or gauge theory) in physical space-time [6–8]. With this method, challenging questions about dynamics in quantum phases of matter in a strong coupling regime can be mapped to processes from string theory (or supergravity) that are tractable. Over the last two decades, AdS/CFT has yielded many important insights into the study of QGP [9,10]. One celebrated finding is the universality of the ratio of shear viscosity to entropy density, $\eta/s \geq 1/4\pi$, for all quantum field theories (including QGP) [11,12]. This lower bound turns out to be consistent with RHIC data [13]. Moreover, the entropy density of a $\mathcal{N} = 4$ super Yang–Mills (SYM) plasma normalized by its Stefan–Boltzmann limit equals 3/4 [14], which is close to its counterpart extracted from lattice quantum chromodynamics (QCD). For more on AdS/CFT and its application in the study of QGP, see [9,10].

Motivated by these similarities, Liu, Rajagopal and Wiedemann computed the screening length of a $Q\bar{Q}$ pair in the presence of a hot wind for $\mathcal{N} = 4$ SYM plasma [15]. Therein, they define the screening length L_s based upon an analysis of a fundamental Wilson loop describing the dynamics of a color-singlet $Q\bar{Q}$ dipole moving with a constant velocity v in the plasma. Specifically, they consider a fundamental string with both of its ends attached to the boundary of the space-time in a boosted background. When the separation L of the $Q\bar{Q}$ pair goes beyond L_s, i.e., the maximum value of L, quark and antiquark become detached from each other with no binding energy, so they will be screened in the QGP. It is known that the binding energy of a $Q\bar{Q}$ pair can be extracted from the thermal expectation value of the Wilson loop [16–18], so by evaluating this Wilson loop, one can compute the binding energy as well as the screening length in a boosted background. After [15], there have been many further generalizations in this direction. For instance, the L_s with respect to the direction of plasma winds was studied in [19]. The back-reaction effect on L_s was investigated in [20]. The L_s of quark–monopole in $\mathcal{N} = 4$ SYM was analyzed in [21]. The R^2 corrections on L_s appeared in [22]. Other relevant results can be found in [23–30].

In this paper we extend the holographic studies of screening length [15] to the case of non-commutative Yang–Mills (NCYM) theories. Because in heavy ion collisions, espe-

[a] e-mail: wupp@hpu.edu.cn
[b] e-mail: xrongzhu@zjhu.edu.cn
[c] e-mail: zhangzq@cug.edu.cn (corresponding author)

Published online: 19 December 2024

cially in noncentral heavy ion collisions, QGP is likely to be subject to a strong magnetic field [31], and this strong magnetic field may affect the dynamical [32–35] and topological [36–38] properties of the QGP, non-commutativity can be considered as a way to model the magnetic fields in heavy ion collisions [39]. In addition, understanding holography in NCYM theories is by itself an interesting endeavor [40–43]. For these reasons, there are several observables or quantities that have already been investigated in NCYM theories. For example, the shear viscosity of the non-commutative plasma was discussed in [44], and the results showed that the shear viscosity takes the universal value $\eta/s = 1/4\pi$, even in the anisotropic situation presented by the non-commutative theory. Subsequently, the jet quenching parameter [45–47], drag force [48–50], Schwinger effect [51], imaginary potential and entropic force [52], and R charge diffusion rates [53] were also studied in NCYM theories. Inspired by this, in this paper we study the screening length of a heavy $Q\bar{Q}$ pair in NCYM theories. More specifically, we want to understand how non-commutativity affects the screening length of a $Q\bar{Q}$ pair as well as quarkonium dissociation in the presence of a hot wind. This is the purpose of the present work.

The paper is structured as follows: In the next section, we briefly introduce the supergravity background dual to NCYM theories presented in [44]. In Sect. 3, we investigate the screening length of a heavy $Q\bar{Q}$ pair moving in this background and consider the axis of the $Q\bar{Q}$ pair along different directions. Our conclusion and discussion are presented in Sect. 4.

2 Setup

It has been argued [40–43] that non-commutative gauge theories at strong coupling could be obtained from string theory by considering the decoupling limit in a system of D_p branes with a background Neveu–Schwarz (NS) B field, which will result in a certain scale of non-commutativity in the large N limit. If we concentrate on the one representing a finite-temperature QFT with a non-commutative plane along space-like directions, e.g. (y, z), the metric (in the string frame) can be written as [44]

$$\begin{aligned} ds^2 = {} & H^{-1/2}\left(-f dt^2 + dx^2 + h\left(dy^2 + dz^2\right)\right) \\ & + H^{1/2}\left(\frac{dr^2}{f} + r^2 d\Omega_5^2\right), \end{aligned} \tag{1}$$

with

$$H = \frac{R^4}{r^4}, \quad f = 1 - \frac{r_h^4}{r^4}, \quad h = \frac{1}{1 + \Theta^2 H^{-1}}, \tag{2}$$

where the constant R denotes the AdS radius; r is the fifth-dimensional coordinate, with $r = \infty$ the boundary and $r = r_h$ the event horizon; Θ stands for the non-commutative parameter; $d\Omega_5$ represents the element of the solid angle of S^5; and (t, x) are the usual commutative directions, while (y, z) exhibit a non-commutative nature. Moreover, due to the presence of the non-commutativity along (y, z), the full SO(3) symmetry of the boundary theory will reduce to SO(2), leaving the rotational invariance only over the (y, z) plane.

The Hawking temperature and entropy density are

$$T = \frac{r_h}{\pi R^2}, \quad s = \frac{N^2\pi^2 T^3}{2}, \tag{3}$$

so one can see that T and s are independent of Θ. For more information about NCYM theory, please refer to [40–44].

3 Screening length in NCYM theories

The screening length L_s of a $Q\bar{Q}$ pair that moves through $\mathcal{N} = 4$ SYM plasma was first computed in [15], where L_s is defined as the maximum value of L in the presence of a hot wind. To simulate a hot wind, one may assume that the plasma is at rest and the reference is boosted with a constant speed. Correspondingly, in the dual theory, the background metric is assumed to be boosted by rapidity. For our scenario, the background metric (1) contains non-commutative and commutative directions. Also, one will consider the metric moving in some directions, so there are many cases for the axis of $Q\bar{Q}$ with respect to non-commutative or commutative directions. To simplify the discussion, we consider just five cases of L: The first one, $L_\perp$, is for (1) moving along the x direction (usual commutative direction), while the $Q\bar{Q}$'s axis is placed in the y or z direction (non-commutative direction). The second is $L_{||}$, which is for the (1) moving along the x direction while the $Q\bar{Q}$'s axis is placed in the same direction. The third and fourth are $L^n_{\perp,1}$ and $L^n_{\perp,2}$, which correspond to (1) moving along the y direction while the $Q\bar{Q}$'s axis is placed in the x direction and the z direction, respectively. By analogy, the fifth is $L^n_{||}$, not described in words here. Next, we follow the argument in [15] to analyze the above five cases of L one by one.

3.1 $L_\perp$ and $L_{||}$

First, we analyze $L_\perp$ and $L_{||}$ by considering the background metric (1) moving along the x direction, so that

$$\begin{aligned} dt &= dt' \cosh\beta - dx' \sinh\beta, \\ dx &= -dt' \sinh\beta + dx' \cosh\beta, \end{aligned} \tag{4}$$

where β is the rapidity parameter and is related to the speed v by $\sinh\beta = \frac{v}{\sqrt{1-v^2}}$.

Substituting (4) into (1) and dropping the primes, one has

$$ds^2 = H^{-1/2}[(-f\cosh^2\beta + \sinh^2\beta)dt^2$$

$$+2\sinh\beta\cosh\beta(f-1)\mathrm{d}t\mathrm{d}x$$
$$+(-f\sinh^2\beta+\cosh^2\beta)\mathrm{d}x^2+h(\mathrm{d}y^2+\mathrm{d}z^2)]$$
$$+H^{1/2}f^{-1}\mathrm{d}r^2. \tag{5}$$

For $L_\perp$, the $Q\bar{Q}$'s axis is along the transverse direction, say the z direction. The string configuration is

$$\tau=t,\quad \sigma=z,\quad x=y=0,\quad r=r(\sigma), \tag{6}$$

and the boundary conditions are

$$r\left(\sigma=\pm\frac{L}{2}\right)=\infty,\quad r(\sigma=0)=r_c,\quad \dot{r}(\sigma=0)=0, \tag{7}$$

with $\dot{r}=\mathrm{d}r/\mathrm{d}\sigma$ and L being the separation between $Q\bar{Q}$.

The string dynamics are described by the Nambu–Goto (NG) action,

$$S_{NG}=-\frac{1}{2\pi\alpha'}\int\mathrm{d}\tau\mathrm{d}\sigma\mathcal{L}=-\frac{1}{2\pi\alpha'}\int\mathrm{d}\tau\mathrm{d}\sigma\sqrt{-detg_{\alpha\eta}}, \tag{8}$$

where

$$g_{\alpha\eta}=G_{\mu\nu}\frac{\partial X^\mu}{\partial\sigma^\alpha}\frac{\partial X^\nu}{\partial\sigma^\eta}, \tag{9}$$

with $G_{\mu\nu}$ the metric and X^μ the target space coordinate.

By means of (5) and (6), the Lagrangian density in (8) reads

$$\mathcal{L}=\sqrt{H^{-1}h(f\cosh^2\beta-\sinh^2\beta)+\left(\cosh^2\beta-\frac{\sinh^2\beta}{f}\right)\dot{r}^2}. \tag{10}$$

Because (10) does not depend on σ explicitly, one can construct a Hamiltonian-like function as a constant of motion,

$$\mathcal{L}-\frac{\partial\mathcal{L}}{\partial\dot{r}}\dot{r}=E. \tag{11}$$

It is pointed out that E labels the possible analytical solutions of strings with fixed Θ and β, such that the results can be presented in the form of L as a function of E for different combinations of Θ and β.

Next, from (10) and (11), one has

$$\dot{r}^2=\frac{a(r)[a(r)-E^2]}{b(r)E^2}, \tag{12}$$

with

$$a(r)=H^{-1}h(f\cosh^2\beta-\sinh^2\beta),$$
$$b(r)=\cosh^2\beta-\frac{\sinh^2\beta}{f}. \tag{13}$$

From (12), one finds that r has two extrema: The first extrema r_{c1} satisfies

$$a(r_{c1})=0, \tag{14}$$

with $a(r_{c1})=a(r)|_{r=r_{c1}}$. But if this condition is met, the string will break down into two separate strings, corresponding to a pair of free quarks with no binding energy, and is thus not considered here.

The other extrema, r_{c2}, satisfies

$$a(r_{c2})-E^2=0, \tag{15}$$

with $a(r_{c2})=a(r)|_{r=r_{c2}}$. It is natural to think that $\dot{r}^2$ switches signs at $a(r_{c2})=a(r_c)$. Thus, r_c can be regarded as a physical turning point of the string configuration.

With fixed Θ, β and E, one can determine r_c by solving (15). Then, by integrating (12), one has

$$L_\perp=2E\int_{r_c}^{\infty}\mathrm{d}r\sqrt{\frac{b(r)}{a^2(r)-a(r)E^2}}, \tag{16}$$

where we have set R as unit. After computing $L_\perp$, one can obtain $L_{s,\perp}$ by reading the maximum value of $L_\perp$.

For $L_{s,||}$, the $Q\bar{Q}$'s axis is along the x direction and the string configuration is

$$\tau=t,\quad \sigma=x,\quad y=z=0,\quad r=r(\sigma). \tag{17}$$

Likewise, the Lagrangian density in (8) becomes

$$\mathcal{L}=\sqrt{H^{-1}f+\left(\cosh^2\beta-\frac{\sinh^2\beta}{f}\right)\dot{r}^2}, \tag{18}$$

yielding

$$L_{||}=2E\int_{r_c}^{\infty}\mathrm{d}r\sqrt{\frac{b_1(r)}{a_1^2(r)-a_1(r)E^2}}, \tag{19}$$

with

$$a_1(r)=H^{-1}f,\quad b_1(r)=\cosh^2\beta-\frac{\sinh^2\beta}{f}. \tag{20}$$

It can be seen that (19) is independent of Θ. This is easy to explain: For $L_{||}$, the metric is moving along the x direction, and the $Q\bar{Q}$'s axis is also along the x direction, implying that the non-commutative effect (related to the (y,z) plane) is not included. So $L_{||}$ naturally equals L_{SYM}.

Before numerical computation, we discuss the value of Θ. There have been various disparate experimental bounds on Θ from different physical considerations; for example, the range is reputed to be (1–10 TeV)$^{-2}$ [54], (10^{12}–10^{13} GeV)$^{-2}$ [55], or (10^{15} GeV)$^{-2}$ [56]. One can see that for these cases, the values of Θ are very small, so there is little hope of getting a significant non-commutative correction in current experiments [44]. But it was shown [40–43] that non-commutativity can introduce a non-locality in space due to space uncertainty, and the non-local effects will be enhanced with the increase in temperature. Thus, the non-commutative effect may be discovered in forthcoming high-energy physics experiments. For convenient analysis,

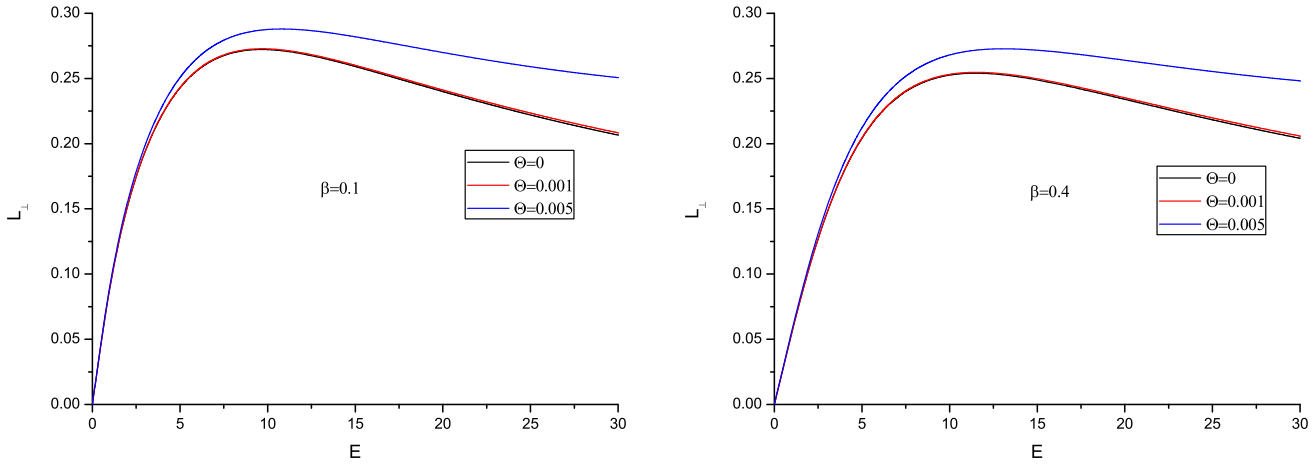

Fig. 1 The separation $L_\perp$ between $Q\bar{Q}$ as a function of the constant of motion E. Left: $\beta = 0.1$; right: $\beta = 0.4$. In both panels from top to bottom, $\Theta = 0.005, 0.001, 0\ GeV^{-2}$, respectively. Here we take $T = 1$

we choose $\Theta = 0.001, 0.005$ GeV^{-2} here, as follows from [52].

In Fig. 1, we plot $L_\perp$ as a function of E for some values of Θ and β, where the left panel is for $\beta = 0.1$ while the right is for $\beta = 0.4$. In both panels, from top to bottom, $\Theta = 0.005, 0.001, 0$ GeV^{-2}, respectively (note that we mainly consider the qualitative results with fixed T, so we simply take $T = 1$ here, similar to [20]). Other cases of different values of Θ and β have similar results. From these figures, one finds that for $E = 0$, there is no $L_\perp$. For finite E, $L_\perp$ first increases until it reaches a maximum value, and then decreases. Physically, a $Q\bar{Q}$ pair will melt with no binding energy if they are separated beyond this maximum value.

Moreover, by comparing the two panels, one sees that as β increases, $L_\perp$ decreases, implying that the greater the velocity, the less screening length is allowed for $Q\bar{Q}$. Further, $Q\bar{Q}$ will melt more easily in the presence of a hot wind, in agreement with the findings of the entropic force [57] and imaginary potential [58,59]. Moreover, from both panels, one can see that as Θ increases, $L_\perp$ increases; that is, the inclusion of non-commutativity increases $L_{s,\perp}$.

We must explain that we do not show the results of $L_{||}$ here, since $L_{||} = L_{SYM}$. Also, $L_\perp$, $L^n_{\perp,1}$, $L^n_{\perp,2}$, and $L^n_{||}$ will revert to L_{SYM} if one turns off the non-commutative effect by taking $\Theta = 0$ in (1). In the next subsection, we will investigate how non-commutativity modifies $L^n_{\perp,1}$, $L^n_{\perp,2}$, and $L^n_{||}$, as well as the corresponding screening length.

3.2 $L^n_{\perp,1}$, $L^n_{\perp,2}$, and $L^n_{||}$

Next, we analyze $L^n_{\perp,1}$, $L^n_{\perp,2}$, and $L^n_{||}$ by considering (1) moving along the y direction,

$$\begin{aligned} \mathrm{d}t &= \mathrm{d}t' \cosh\beta - \mathrm{d}y' \sinh\beta, \quad \mathrm{d}y \\ &= -\mathrm{d}t' \sinh\beta + \mathrm{d}y' \cosh\beta. \end{aligned} \tag{21}$$

Substituting (21) into (1) and dropping the primes, one gets

$$\begin{aligned} \mathrm{d}s^2 = H^{-1/2}[&(-f\cosh^2\beta + h\sinh^2\beta)\mathrm{d}t^2 \\ &+2\sinh\beta\cosh\beta(f-h)\mathrm{d}t\mathrm{d}x \\ &+\mathrm{d}x^2 + (-f\sinh^2\beta + h\cosh^2\beta)\mathrm{d}y^2 \\ &+h\mathrm{d}z^2] + H^{1/2}f^{-1}\mathrm{d}r^2. \end{aligned} \tag{22}$$

The next analysis process is similar to the previous subsection, so we just show the final results. We find

$$L^n_{\perp,1} = 2E\int_{r_c}^{\infty} \mathrm{d}r \sqrt{\frac{B(r)}{A^2(r) - A(r)E^2}}, \tag{23}$$

with

$$\begin{aligned} A(r) &= H^{-1}[f\cosh^2\beta - \sinh^2\beta \\ &\quad + \cosh^2\beta\sinh^2\beta(f-h)^2], \\ B(r) &= \cosh^2\beta - \frac{h\sinh^2\beta}{f}. \end{aligned} \tag{24}$$

$$L^n_{\perp,2} = 2E\int_{r_c}^{\infty} \mathrm{d}r \sqrt{\frac{B_1(r)}{A_1^2(r) - A_1(r)E^2}}, \tag{25}$$

with

$$\begin{aligned} A_1(r) &= H^{-1}h(f\cosh^2\beta - h\sinh^2\beta), \\ B_1(r) &= \cosh^2\beta - \frac{h\sinh^2\beta}{f}. \end{aligned} \tag{26}$$

$$L^n_{||} = 2E\int_{r_c}^{\infty} \mathrm{d}r \sqrt{\frac{B_2(r)}{A_2^2(r) - A_2(r)E^2}}, \tag{27}$$

with

$$\begin{aligned} A_2(r) = H^{-1}&(f\cosh^2\beta - \sinh^2\beta) \\ &\times(-f\sinh^2\beta + h\cosh^2\beta), \end{aligned}$$

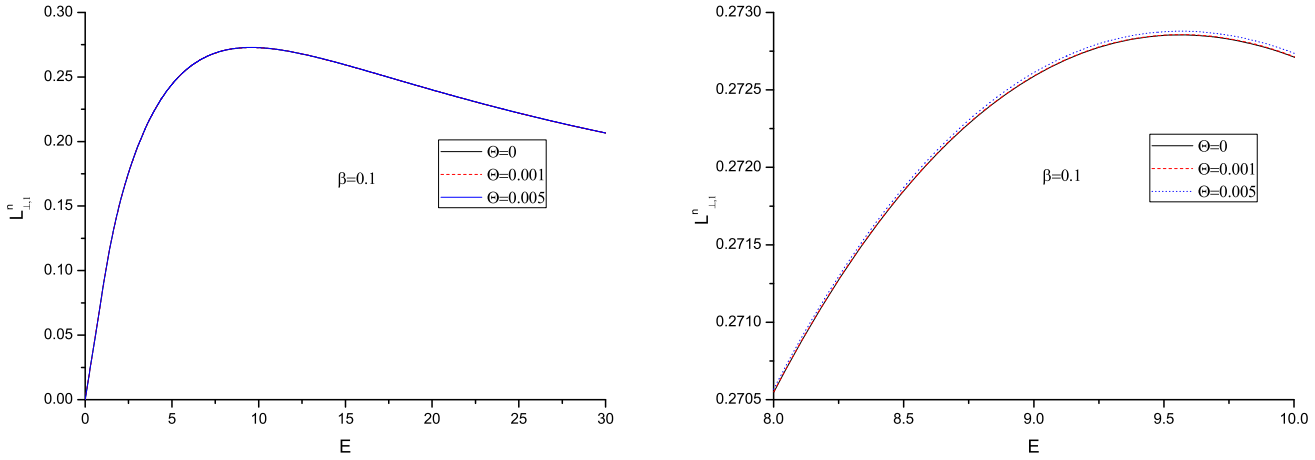

Fig. 2 $L^n_{\perp,1}$ versus E. Left: complete graph. Right: local image. In both panels, from top to bottom, $\Theta = 0.005, 0.001, 0$ GeV^{-2}, respectively. Here we take $T = 1$, $\beta = 0.1$

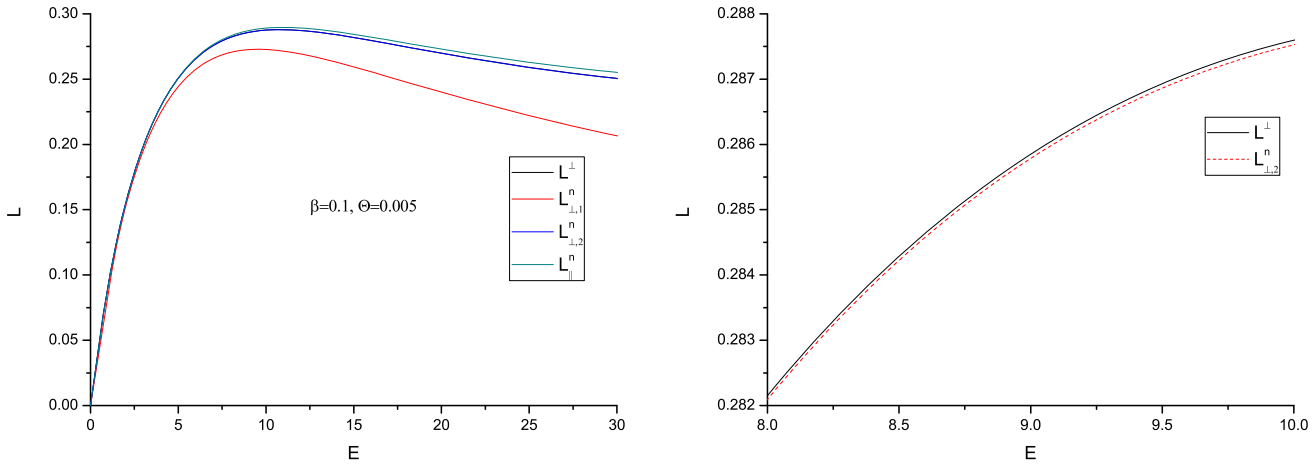

Fig. 3 Left:$L^n_{\perp,2}$ versus E; Right: $L^n_{||}$ versus E. In both panels, from top to bottom, $\Theta = 0.005, 0.001, 0\ GeV^{-2}$, respectively. Here we take $T = 1$, $\beta = 0.1$

$$B_2(r) = \cosh^2\beta - \frac{h\sinh^2\beta}{f}. \tag{28}$$

In Fig. 2, we plot $L^n_{\perp,1}$ against E with fixed $\beta = 0.1$, where the left panel is the complete graph while the right is the local image. From the left panel, one sees that the results of $L^n_{\perp,1}$ with different values of Θ are very close. To distinguish these figures, we plot the local image on the right. One can see that as Θ increases, $L^n_{\perp,1}$ increases slightly. Although the effect is not obvious, the result is consistent with previous findings of $L_\perp$. In Fig. 3, we plot two other cases, where the left panel is for $L^n_{\perp,2}$ versus E and the right is for $L^n_{||}$ versus E. One can see that in both cases, the results are consistent: increasing Θ leads to increasing screening length.

In order to compare the four cases (actually, there are five cases; the fifth is $L_{||} = L_{SYM}$, smaller than the other four), we plot Fig. 4, where the left panel is the complete graph and the right is the local image. Together, from the results of both panels, we find

$$L^n_{s,||} > L_{s,\perp} > L^n_{s,\perp,2} > L^n_{s,\perp,1} > L_{s,||} = L_{s,SYM}. \tag{29}$$

These are the main findings of the present work. The physical interpretation of the results will be discussed in the next section.

4 Conclusion and discussion

From the AdS/CFT point of view, a heavy $Q\bar{Q}$ pair described by a Wilson loop can be defined as an open string with both of its ends attached to the boundary of the space-time. Evaluating the Wilson loop can teach us about the L-dependent $Q\bar{Q}$ potential [16–18] and, hence, the screening length of $Q\bar{Q}$ in the presence of a hot wind [15]. In this paper, we studied the screening length of a $Q\bar{Q}$ pair moving in strongly coupled NCYM plasma. We performed the analysis by computing

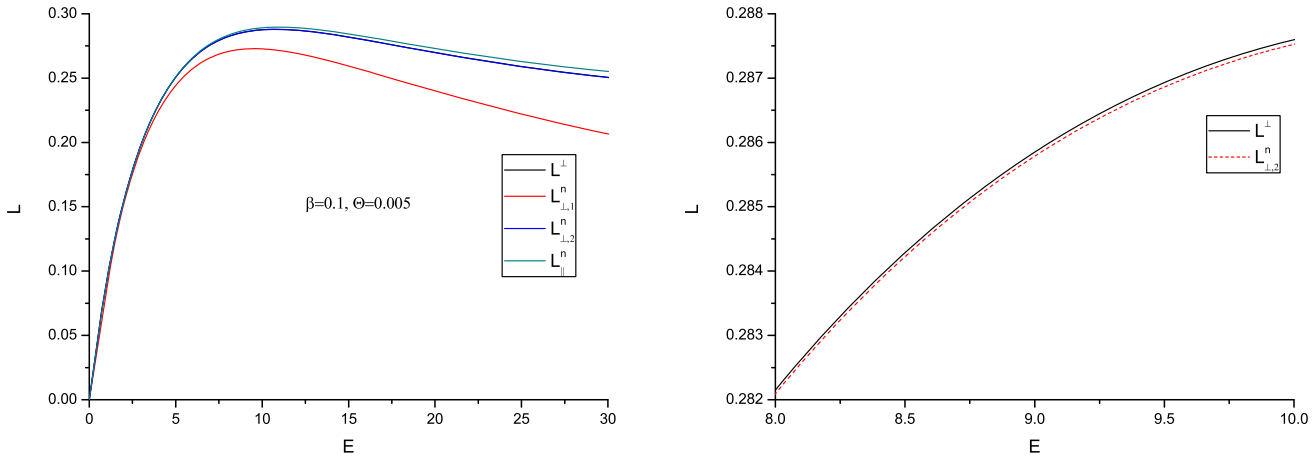

Fig. 4 $L_\perp$, $L^n_{\perp,1}$, $L^n_{\perp,2}$, and $L^n_{||}$ versus E. Left: complete graph. Top to bottom, $L^n_{||}$, $L_\perp$, $L^n_{\perp,2}$, $L^n_{\perp,1}$, respectively. Right: local image of $L_\perp$ and $L^n_{\perp,2}$. Here we take $T = 1$, $\beta = 0.1$, $\Theta = 0.005$

the Wilson loop in a boosted background and considered the $Q\bar{Q}$'s axis located in various directions. It was shown that the inclusion of non-commutativity tends to increase the screening length, thus enhancing the binding energy of $Q\bar{Q}$. Furthermore, non-commutativity reduces quarkonium dissociation, in agreement with previous findings of the imaginary potential and entropic force [52].

Specifically, we found the relation (29). To facilitate understanding, we turn (29) into the following relation:

$$(y, y) > (x, z) > (y, z) > (y, x) > (x, x) = SYM, \quad (30)$$

where the first letter in the parentheses denotes the moving direction of the background metric and the second one represents the direction of $Q\bar{Q}$'s axis. The maximum (y, y) or (z, z) tells us that the non-commutative effect will evidently appear when the $Q\bar{Q}$'s axis and metric's direction of motion are along the same non-commutative direction. Also, from (30), one infers that when the $Q\bar{Q}$'s axis is placed along the non-commutative direction, the non-commutative effect becomes rather obvious. In other words, for the non-commutative effect, the direction of the metric's movement is less important than that of the $Q\bar{Q}$'s axis. This conclusion can also be deduced from the other two details. The first is for (y,x) (see Fig. 2): the results of $L^n_{\perp,1}$ with different values of Θ are very close. This should make sense since the $Q\bar{Q}$'s axis is along the x direction, not the non-commutative direction. The second is that (x, z) and (y, z) are very close (see Fig. 4). This is also easy to understand. In both cases, whether the background moves along the y direction or the x direction, the $Q\bar{Q}$'s axis is along a non-commutative direction.

Here, we would like to compare our results with others. In [48], the author argued that the drag force is reduced by the effect of non-commutativity, so the non-commutativity reduces the viscous force. As we know, a stronger force implies a more strongly coupled medium, closer to an ideal liquid. Therefore, the presence of non-commutativity reduces the viscous force; thus, QGP becomes less like an ideal liquid. Together with our results, one can conclude that $Q\bar{Q}$ will melt less easily when the viscous force is reduced. Conversely, $Q\bar{Q}$ will melt more easily when the viscous force is increased. In other words, $Q\bar{Q}$ will melt more easily in more "perfect" strongly coupled plasma, consistent with the findings of the screening length in the Gauss–Bonnet background [22].

Finally, we want to point out that we considered only five extremes of the screening length; actually, one should consider different orientations of the velocity with respect to the direction of $Q\bar{Q}$'s axis. Also, it would be interesting to study the screening length in NCYM theories in different dimensions. We hope to make progress in this regard in our future work.

Acknowledgements This work is supported by the National Natural Science Foundation of China (NSFC) under Grant nos. 12375140, 12035006 and the Ministry of Science and Technology under Grant no. 2020YFE0202001.

Data Availability Statement This manuscript has no associated data. [Author's' comment: This is a theoretical study and no experimental data has been listed.]

Code Availability Statement This manuscript has no associated code/software. [Author's comment: Code/Software sharing not applicable to this article as no code/software was generated or analysed during the current study.]

Funded by SCOAP[3].

References

1. J. Adams et al. [STAR Collaboration], Nucl. Phys. A **757**, 102 (2005)
2. K. Adcox et al. [PHENIX Collaboration], Nucl. Phys. A **757**, 184 (2005)
3. E.V. Shuryak, Nucl. Phys. A **750**, 64 (2005)
4. U.W. Heinz, R. Snellings, Annu. Rev. Nucl. Part. Sci. **63**, 123–151 (2013)
5. S. Ryu, J.-F. Paquet, C. Shen, G.S. Denicol, B. Schenke, S. Jeon, C. Gale, Phys. Rev. Lett. **115**, 132301 (2015)
6. J.M. Maldacena, Adv. Theor. Math. Phys. **2**, 231 (1998)
7. S.S. Gubser, I.R. Klebanov, A.M. Polyakov, Phys. Lett. B **428**, 105 (1998)
8. O. Aharony, S.S. Gubser, J. Maldacena, H. Ooguri, Y. Oz, Phys. Rep. **323**, 183 (2000)
9. J.C. Solana, H. Liu, D. Mateos, K. Rajagopal, U.A. Wiedemann, arXiv:1101.0618
10. O. DeWolfe, S.S. Gubser, C. Rosenc, D. Teaney, Prog. Part. Nucl. Phys. **75**, 86 (2014)
11. G. Policastro, D.T. Son, A.O. Starinets, Phys. Rev. Lett. **87**, 081601 (2001)
12. P. Kovtun, D.T. Son, A.O. Starinets, Phys. Rev. Lett. **94**, 111601 (2005)
13. M. Luzum, P. Romatschke, Phys. Rev. C **78**, 034915 (2008)
14. S. Gubser, I.R. Klebanov, A. Peet, Phys. Rev. D **54**, 3915 (1996)
15. H. Liu, K. Rajagopal, U.A. Wiedemann, Phys. Rev. Lett. **98**, 182301 (2007)
16. J.M. Maldacena, Phys. Rev. Lett. **80**, 4859 (1998)
17. S.-J. Rey, S. Theisen, J.-T. Yee, Nucl. Phys. B **527**, 171 (1998)
18. A. Brandhuber, N. Itzhaki, J. Sonnenschein, S. Yankielowicz, Phys. Lett. B **434**, 36 (1998)
19. M. Natsuume, T. Okamura, JHEP **09**, 039 (2007)
20. S. Chakraborttya, T.K. Dey, JHEP **05**, 094 (2016)
21. W.-S. Xu, D.F. Zeng, Nucl. Phys. B **890**, 228 (2015)
22. Z.Q. Zhang, X.R. Zhu, Phys. Lett. B **853**, 138676 (2024)
23. C. Krishnan, JHEP **12**, 019 (2008)
24. C. Athanasiou, H. Liu, K. Rajagopal, JHEP **05**, 083 (2008)
25. S.J. Sina, Y. Zhou, JHEP **05**, 044 (2009)
26. J. Sadeghi, S. Heshmatian, Int. J. Theor. Phys. **49**, 1811 (2010)
27. A.N. Atmaja, H.A. Kassim, N. Yusof, Eur. Phys. J. C **75**, 565 (2015)
28. X.R. Zhu, P.-P. Wu, Z.Q. Zhang, Eur. Phys. J. A **60**, 35 (2024)
29. E. Caceres, M. Natsuume, T. Okamura, JHEP **0610**, 011 (2006)
30. M. Chernicoff, J.A. Garcia, A. Guijosa, JHEP **09**, 068 (2006)
31. D.E. Kharzeev, L.D. McLerran, H.J. Warringa, Nucl. Phys. A **803**, 227 (2008)
32. K.A. Mamo, JHEP **05**, 121 (2015)
33. D. Dudal, D.R. Granado, T.G. Mertens, Phys. Rev. D **93**, 125004 (2016)
34. Z. Fang, Phys. Lett. B **758**, 1 (2016)
35. R. Rougemont, R. Critelli, J. Noronha, Phys. Rev. D **93**, 045013 (2016)
36. K. Fukushima, D.E. Kharzeev, H.J. Warringa, Phys. Rev. D **78**, 074033 (2008)
37. D.T. Son, A.R. Zhitnitsky, Phys. Rev. D **70**, 074018 (2004)
38. D.E. Kharzeev, H.U. Yee, Phys. Rev. D **83**, 085007 (2011)
39. V.P. Gusynin, V.A. Miransky, I.A. Shovkovy, Phys. Rev. D **52**, 4747 (1995)
40. N. Seiberg, E. Witten, JHEP **9909**, 032 (1999)
41. A. Hashimoto, N. Itzhaki, Phys. Lett. B **465**, 142 (1999)
42. J.M. Maldacena, J.G. Russo, JHEP **9909**, 025 (1999)
43. M. Alishahiha, Y. Oz, M.M. Sheikh-Jabbari, JHEP **9911**, 007 (1999)
44. K. Landsteiner, J. Mas, JHEP **0707**, 088 (2007)
45. S. Chakraborty, S. Roy, Phys. Rev. D **85**, 046006 (2012)
46. J. Sadeghi, B. Pourhassan, Acta Phys. Polon. B **43**, 1825 (2012)
47. M.A. Akbari, arXiv:1104.4924 [hep-th]
48. S. Roy, Phys. Lett. B **682**, 93 (2009)
49. K.L. Panigrahi, S. Roy, JHEP **04**, 003 (2010)
50. T. Matsuo, D. Tomino, W.Y. Wen, JHEP **0610**, 055 (2006)
51. U.N. Chowdhury, Adv. High Energy Phys. **2021**, 6648322 (2021)
52. Z.Q. Zhang, X.R. Zhu, P.P. Wu, Nucl. Phys. B **945**, 114689 (2019)
53. D. Roychowdhury, JHEP **07**, 121 (2015)
54. S.M. Carroll, J.A. Harvey, V.A. Kostelecky, C.D. Lane, T. Okamoto, Phys. Rev. Lett. **87**, 141601 (2001)
55. A. Anisimov, T. Banks, M. Dine, M. Graesser, Phys. Rev. D **65**, 085032 (2002)
56. I. Mocioiu, M. Pospelov, R. Roiban, Phys. Lett. B **489**, 390 (2000)
57. K.B. Fadafan, S.K. Tabatabaei, Phys. Rev. D **94**, 026007 (2016)
58. S.I. Finazzo, J. Noronha, JHEP **01**, 051 (2015)
59. M. Ali-Akbari, D. Giataganas, Z. Rezaei, Phys. Rev. D **90**, 086001 (2014)